ORIGINAL PAPER

Biocompatible nano-bandage modified with silver nanoparticles based on herbal for burn treatment

Rozhin Karami[1] · **Pouran Moradipour**[2,3] · **Elham Arkan**[3] · **Reza Zarghami**[1] · **Khodabakhsh Rashidi**[4] · **Elahe Darvishi**[5]

Abstract

Electrospinning has garnered much attention for skin renewal, emphasizing skin's pivotal role as a primary protective layer and the susceptibility to loss caused by burns. The research aimed to develop a multipurpose wound dressing that safeguard injuries and facilitates the renewal of dermal tissues. Two-layer nanofibers were prepared using polyvinyl alcohol–chitosan–gelatin/polyacrylonitrile (PVA–CS–Gel/PAN), containing mupirocin (Mu 3% w/w) in underlying layer and silver nanoparticles (AgNps) in the upper layer with varying concentrations. AgNps were synthesized from *Capsella bursa-pastoris* extract by the green method and characterized using XRD, SEM, FTIR, and UV techniques. Then, PVA–CS–Gel/PAN solutions with AgNps and Mu were electrospun into multilayer dressings. The effectiveness of the nanofibers was evaluated through in vitro and in vivo tests. The study examined the nanofibers containing spherical AgNps with an average diameter of 72.57 nm and a negative surface charge (− 12 mv). They had uniform and smooth surfaces with a diameter range of 476.31 to 926.04 nm. According to swelling and contact angle results, hydrophilicity of samples had a direct relation with water absorption. Controlled drug release within 72 h followed Higuchi or first-order profiles. MTT and antibacterial analyses indicated that optimized nanofibers (Mu/1% AgNps) had suitable biocompatibility and synergistic potential against *Escherichia coli* (*E. coli*) and *Staphylococcus aureus* (*S. aureus*) bacteria. Additionally, an in vivo test on rats with second-degree burns after 28 days demonstrated a 98.97% improvement in revival, outperforming its commercial counterparts. Consequently, the results position the designed composite nanofiber as a promising candidate for wound healing applications, aiding in enhancing skin regeneration.

Keywords Electrospun nanofibers · Wound dressing · Green synthesis · Silver nanoparticles · Mupirocin · *Capsella bursa-pastoris*

Extended author information available on the last page of the article

Introduction

The skin serves as a vital protective layer enveloping the outer surface of the human body [1–3], playing a crucial role in preserving homeostasis and safeguarding against the intrusion of microorganisms [4]. Among diverse wounds, skin burn injuries present formidable treatment challenges due to the complexity of their recovery mechanisms. The associated pain and overall impact on individuals experiencing these injuries are unparalleled compared to other wound types [5, 6]. Hence, wound healing has become a significant health issue with considerable global medical importance [7]. The process generally consists of successive stages: hemostasis, inflammation, cell migration, proliferation, and ultimately remodeling [2, 6–15].

Treatment approaches vary based on burn types; thus, an initial important step in treatment involves accurately determining the degree of the burn [16]. Traditional skin substitutes (autografts, xenografts, and allografts) face limitations in treating damaged skin due to issues like enzymatic resistance, antigenicity, and limited donors. Subsequently, recent researches have focused on advanced wound dressing materials that shield and expedite healing [17]. These dressings act as sterile barriers, aiding in surface protection, bacteriostatic control, reducing necrosis, and shortening the recovery period, designed to be permeable and biocompatible [7, 18].

Nanofibers, beyond their conventional dressing roles, provide a positive environment, fulfilling the required characteristics for wound dressings [7, 17]. Several manufacturing techniques, such as melt blowing, rotary jet spinning, mechanical drawing, pressure spinning, template synthesis, phase separation, self-assembly, and electrospinning, have been developed for producing nanofiber scaffolds [17, 19]. However, many of these methods have drawbacks, including complex procedures, unsuitability for specific polymers, and a lack of control over fiber diameter and direction [19]. Among these approaches, the electrospinning stands out as a superior method, recognized for its low cost, high speed, and ease of use [20–23]. Nevertheless, its principal disadvantages include low productivity and the requirement for a high operating voltage [7, 17].

Despite these limitations, it is versatile for creating precisely controlled biological fibers using a range of polymers, applicable in sensor technology, filtration, textiles, protective wear, drug delivery, and wound dressing [1, 9, 11, 14, 17, 19–22, 24–26]. Moreover, electrospun membranes possess distinctive properties, including high surface area/volume ratio for efficient loading of agents, a structure resembling the extracellular matrix (ECM), mechanical stability, air permeability, moisture balance, effective exudate absorption, and the ability to release active substances. They also provide an ideal microenvironment for cellular processes, prevent microbe infiltration, aid in homeostasis, and contribute to scar healing [1, 4, 9, 11, 14, 15, 17, 20–22, 24–27].

Utilizing a combination of various natural and synthetic polymers can enhance the scaffolding's resemblance to the body's natural tissue by modifying its strength, biological activity, and degradation rate [9, 23, 28–33]. Gelatin (Gel)

is a biomaterial that has been extensively studied for use in cell scaffolding and wound dressings due to its similarity to ECM structure of the skin. Gelatin chains are rich in Arginylglycylaspartic acid (RGD) peptide, enhancing cell adhesion to the scaffold's surface and potentially accelerating wound healing [13, 26, 33–37]. Chitosan (CS), a natural polysaccharide derived from chitin, is another widely used biopolymer known for its high biocompatibility, biodegradability, antibacterial properties, and non-toxicity [4, 33–38]. The antibacterial effect of CS is primarily associated with the leakage of intracellular substances. It alters cell membrane permeability through the interaction of positive protonated amino groups with the negatively charged bacterial surfaces, leading to the leakage of intracellular substance and bacterial death [7, 17, 27].

However, its polycationic nature, rigid chemical structure, and limited chain entanglement hinder the formation of nanofibers through electrospinning [29, 39]. To overcome the limitations of electrospinning and improve the mechanical properties of biopolymers like CS and Gel, polymers such as polyvinyl alcohol (PVA) are utilized as the base material [29, 36]. PVA is a water-soluble synthetic polymer with favorable physical and chemical properties, extensively employed in medicine, tissue engineering, wound dressing, and drug delivery systems [33, 37, 40–42]. Another suitable option for the treatment of skin disorders is polyacrylonitrile (PAN) [43–46]. It is a typical polar polymer with excellent filtration, distinctive mechanical properties, biocompatibility, the capacity to absorb exudates through proper swelling, and the capability to release desired therapeutic agents. PAN also effectively isolates airborne bacteria and viruses, making it suitable for use as a wound dressing [18, 43–46].

Wounds, particularly secondary burns, are susceptible to bacterial infection, which not only disrupts the regular healing process, but may also lead to deformation of the wound tissue, posing a potential threat to the patient's life [2, 7, 12, 15, 17, 18, 47–49]. Nonetheless, traditional wound dressings, like cotton or gauze, lack crucial antibacterial properties and require frequent changes, risking secondary injury to the wound [39]. Therefore, there is a critical need for scaffolds enabling extended and controlled release of antibacterial drugs for wound dressing. [27]. Mupirocin (Mu) is an antibiotic that specifically binds to ribonucleic acid (tRNA), inhibiting bacterial protein biosynthesis. It performs a vital function in eliminating gram-positive bacteria, such as methicillin-resistant *Staphylococcus aureus*, and facilitates the rapid transfer of healthy tissue to the affected area [32, 50, 51]. In recent decades, there has been significant focus on producing nanofibers with biologically active plant extracts and metallic nanoparticles through electrospinning [52–54].

Notably, silver nanoparticles (AgNps) due to their exceptional antibacterial and anti-inflammatory properties have garnered significant attention [17, 55–61]. For instance, Chen et al. produced nanofibrous PAN incorporating various amounts of Curcumin (Cur), tannic acid, and AgNps. The release of AgNps, in addition to Cur, resulted in enhanced antimicrobial properties in the obtained Ag/polymer composite membranes [18]. Diverse recognized methods, encompassing chemical, physical, and photochemical routes, are used for synthesizing AgNps. However, these approaches necessitate extended processing times, high energy consumption, elevated operating costs, and present potential environmental hazards, rendering them

inefficient and restrictive in practical applications [18, 55, 57–59, 62–70]. Recently, the usage of biological techniques for synthesizing AgNps using substances derived from plants has increased. This is attributed to the therapeutic properties of bioactive molecules found in plants, making this method both environmentally friendly and cost-effective. [18, 55, 57–59, 62–69].

As an example, Bozkaya et al. synthesized silver nanoparticles utilizing *Centella asiatica* (CA) extract. Cytotoxic and antimicrobial investigations revealed that CA-AgNps-loaded PCL/PEO hybrid nanofibers demonstrated favorable biocompatibility for L929 fibroblast cells and exhibited effectiveness against *Staphylococcus aureus*, *Escherichia coli*, and *Candida albicans* [17]. In another study, Alinezhad Sardareh et al. employed a green method to produce silver nanoparticles using donkey dung extract. These nanoparticles were integrated into Gel and PLA nanofibers, revealing heightened antibacterial performance against both gram-positive and gram-negative species in comparison to PLA and Gel tissues without nanoparticles [7]. The phytochemical constituents in plant extracts function as reducing and stabilizing agents in the synthesis of metal nanoparticles. Indeed, these natural components are essential for the conversion of NO_3^- to NO_2^-, electron transfer to Ag^+ ion, leading to the formation of AgNps [65, 71–74].

Capsella bursa-pastoris, owing to its primary metabolites (organic acids, amino acids, and fatty acids) and secondary ones (phenolic compounds and sterol derivatives), own remarkable properties for preventing bleeding and regulating blood clotting. It is primarily applied as a poultice for addressing superficial inflammations, aiding in the healing of infected wounds, functioning as a hemostatic agent, and serving as an antioxidant to alleviate scars, skin disorders, and eczema. Moreover, this plant, rich in vitamins B and C, contributes to the healing of burn wounds through their positive effects on cell growth and the migration of human skin fibroblasts [75–78].

In this study, for the first time, a dressing incorporating a bilayer nanofiber coated with *Capsella*-AgNps was developed and evaluated for multifunctional wound dressing applications. The scaffolds were designed to assess morphology, physical and chemical properties, swelling, hydrophobicity, drug release, antibacterial features, and in *vitro* biocompatibility with skin fibroblasts. Subsequently, animal tests were conducted to determine the efficacy of the prepared nanofibers in promoting the wound healing process.

Material and methods

Materials

PVA (Mw of 72,000, 98% hydrolyzed), glutaraldehyde (GA), acetic acid, dimethylformamide (DMF), and ethanol 96% were purchased from Merck company. Chitosan (low molecular weight with 90% deacetylation degree), gelatin (Mw of 180.1559), MTT [3-(4, 5-dimethylthiazol-2-yl)-2, 5-diphenyltetrazolium bromide], $AgNO_3$ (Mw of 169.87), FBS (fetal bovine serum), ketamine, and xylazine were purchased from Sigma-Aldrich company. Polyacrylonitrile (Mw of 80,000) was

obtained by Polyacryl Company from Esfahan (Iran). Mupirocin was obtained from Daroupakhsh Pharmaceutical Company in Tehran (Iran). Human fibroblast cells (L929), *Escherichia coli* (*E. coli*) (ATCC 25922), and *Staphylococcus aureus* (*S. aureus*) (ATCC 27853) were prepared from the Pastor Institute of Iran. The aerial organs of *Capsella bursa-pastoris* were collected from farms around Kermanshah city, located in the west of Iran.

Preparation of the aqueous extract of Capsella bursa-pastoris

After collecting *Capsella bursa-pastoris*, the aerial parts of the plant were separated. To remove the mud and possible contaminants, they were washed three times with water and dried at room temperature in an environment free of dust and direct light. Then, 2 g of the plant powder, prepared by an electric grinder, were added to an Erlenmeyer flask containing 100 ml of distilled water at boiling temperature (100 °C) and stirred for 5 min. The extract was centrifuged at 5000 rpm for 15 min. In the last step, the mixture was passed through Whatman filter paper (No.1) to separate the plant extract and remove insoluble matter. The obtained extract was kept at 4 °C for further steps [79, 80].

Green synthesis of silver nanoparticles by Capsella extract

For the reduction of silver ions in the aqueous extract of the plant, various volumes of the extract, consisting of 0.25, 0.5, 1, and 2.5 ml, were added slowly to 5 ml of 1mM silver nitrate solution. Then, all samples were exposed to direct sunlight for 15 min under the same conditions. The color of the extract changed from colorless to yellow, light brown, and finally dark brown due to the reduction of silver ions and the formation of the AgNps [56, 81–84].

The brown AgNps were separated from the solution using a centrifuge at 8000 rpm for 15 min at 4 °C. To remove excess extract and unreacted ions, they were washed with distilled water several times [81]. Finally, the brown-colored solution was dried at 60 °C for 24 h in a vacuum oven. The final dried precipitate was kept at 4 °C for further study [79].

Preparation of multilayers electrospun nanofibers

The suggested wound dressing was constructed with two different layers, including an inner layer (in direct contact with the skin) and an outer layer. The inner layer consisted of PVA, chitosan (CS), and gelatin (Gel) as the basic platform, while the outer layer was made of PAN. To create the inner layer, a solution of 12 wt% of PVA in water ($T = 70$ °C) was prepared. Various concentrations of 0, 0.5, and 1 wt% of the AgNps relative to the dry PVA powder were added to water, sonicated for 15 min, and stirred for 3 h. Then, 3.25 and 1.75 ml of CS 3wt% and Gel 30 wt% solutions in acetic acid were slowly added to the initial PVA solution and stirred for 24 h at ambient temperature. As a final step, mupirocin 3 wt% was added to the solution and stirred for 2 h at a constant speed. For the outer layer, a 13 wt% of PAN solution

in DMF was prepared. Finally, 1 wt% of the AgNps was added to DMF and sonicated for 15 min before adding PAN.

Electrospinning

Two-layer nanofibrous mats were prepared using a dual-pump electrospinning machine (Fanavaran nano-meghyas Co, Iran). A 2-ml PAN solution at room temperature and a relative humidity of 25–30%, under a voltage of 19 kV, a flow rate of 0.5 ml/h, and a distance of 18 cm, was electrospun onto a rotating drum covered with aluminum foil. Subsequently, the mat was placed in a vacuum oven at a temperature of 70 °C for 24 h to eliminate the excess solvent (DMF). Following this, 1 ml of the prepared PVA-CS-Gel solution, under a voltage of 18 kV, a flow rate of 0.5 ml/h, and a distance of 12 cm was gathered onto the previously electrospun PAN mat.

As PVA-CS-Gel nanofiber mats exhibited hydrophilic properties and rapid degradation at ambient temperature, they were exposed to 50% glutaraldehyde vapors in a desiccator for 12 h. After this period, the samples were transferred to an oven at 40 °C for 48 h to enhance the crosslinking rate and remove excess moisture from unsaturated glutaraldehyde for further characterization [85].

Characterization

Physical and chemical characterization

The absorption of the AgNps was investigated using UV–Vis spectroscopy (Shimadzu, Japan) at a wavelength range of 200–800 nm. Field emission scanning electron microscopy (FESEM) analysis was employed to characterize the surface morphology and determine the size of nanoparticles and nanofiber layers, utilizing image analysis with Image software. Fourier transform infrared spectroscopy (FTIR) (Shimadzu, Japan) in the range of 400–4000 cm^{-1} was utilized to examine the chemical bonds and functional groups of both AgNps and nanofibers. The crystal structures of the AgNps was studied using X-ray diffraction spectroscopy (XRD). The dynamic light scattering (DLS) method was applied to ascertain the size distribution and hydraulic radius of the AgNps. Additionally, the surface charge of AgNps was measured using a zeta potential device (ZEN3600, Malvern Co) as an indicator for evaluation the dispersion stability of the samples. The viscosity of the initial polymeric solutions was measured at room temperature using a Brookfield RVPV-II viscometer made in the USA, with spindle number 21, rotation speed 5 rpm, and a duration of 2 min.

Determination of minimum inhibitory and bacterial concentration

The antibacterial properties of the AgNps synthesized against gram-negative *E. coli* and gram-positive *S. aureus* were investigated. Solutions of the AgNps ranging from 100 to 12.5 µg/ml in deionized water were prepared through serial dilutions. Subsequently, culture medium and bacterial suspension, equivalent to 0.5 McFarland

turbidity, were added to each sample. One sample contained bacteria and a culture medium (without nanoparticles), serving as a growth control to determine the turbidity of bacterial growth. Following this, all suspensions were incubated for 24 h at 37 °C. Ultimately, the increased turbidity of each sample, indicating bacterial growth, was examined. Therefore, the lowest concentration of the AgNps that maintained the culture medium transparent was recorded as the minimum inhibitory concentration (MIC) for that bacterium [86, 87].

To determine the minimum bacterial concentration (MBC), the concentration specified for the MIC and concentrations above it were used. For each concentration, a separate loop of the solution one loop of the solution was removed, cultured in nutrient agar medium, and placed in the incubator for 24 h. After this duration, the culture medium was examined, and the concentration of nanoparticles causing the absence of bacterial colonies in the culture medium was recorded as MBC for the intended bacteria [86, 87].

Apparent water contact angle (WCA) measurement and swelling

The wettability of the solution was analyzed using a contact angle measurement device (KURSS, Hamburg, Germany) to explore the hydrophilicity and hydrophobicity behavior of the final electrospun mats [88]. Water absorption was investigated by immersing the samples in a phosphate buffer solution (PBS) with pH = 7.4 at a temperature of 37 °C. At intervals of 1, 3, 5, 12, 24, 48, and 72 h, the samples were taken out of the buffer solution, placed between two sheets of filter paper to remove excess liquid, and then weighed. Equation 1 is used to calculate the inflation percentage of each sample based on the swelling degree (SD) [88, 89]:

$$SD = \frac{W_t - W_i}{W_i} \times 100 \tag{1}$$

where W_t is the weight of the swollen specimens at the test times after hydration by the filter paper, and W_i is the initial weight of the specimens in the dry state.

In vitro drug release and kinetics study

The in vitro release of mupirocin was investigated by the total immersion method. 40 mg of fibers were placed in a dialysis bag (SERVA, MWCO, 12,000 Da), and 2 ml of PBS (pH = 7.4) was added to each bag, acting as the donor solution. The bag was then immersed in 50 ml of the receptor medium (PBS 0.2 M, pH 7.4) and incubated at 37 °C under magnetic stirring. At specified time intervals, 1 ml of the medium was taken, and the same volume of fresh buffer was added. For drug concentration assay, the taken samples were analyzed at 220 nm using a UV spectrophotometer (UVmini-1240, Shimadzu, Germany) [90]. For evaluation, a model-dependent approach was employed to compare the dissolution profile. The release kinetics data were fitted to kinetic models, including the zero-order (Eq. 2), first-order (Eq. 3), and Higuchi matrix (Eq. 4) release equations to find the equation with the best fit [73]:

$$C = Kt \tag{2}$$

$$\text{Log}C = \text{Log}C_0 - Kt/2.303 \tag{3}$$

$$Q = Kt^{1/2} \tag{4}$$

where C_0 is the initial concentration of the drug, K is the zero-order or first-order rate constant, or the Higuchi dissolution constant in the corresponded equations, and Q is the amount of drug released during time t per unit area.

Antibacterial activity

Two bacterial species, *S. aureus* (gram-positive) and *E. coli* (gram-negative), were used to assess the antibacterial properties of the scaffold using the disk diffusion method. Initially, the bacterial strains were incubated at a specific temperature of 37 °C and subjected to an intense and rotational shaking for 24 h to facilitate maximum growth and activity. Afterward, a portion of the bacterial culture was aseptically removed and placed on a solid culture medium containing agar and other sugars, such as glucose broth, linearly and continuously within the plate. Circular disks, each with a diameter of 6–10 mm, were then cut from the sample containing nanofibers, as well as control samples, and positioned in a culture medium for 24 h. The radius of the growth inhibition zone around each disk was examined as a criterion for antibacterial properties [87].

MTT assay

The human fibroblast cell line (L929) was seeded in 96-well plates and incubated with 5% CO_2 at 37 °C until reaching confluency (typically 24 h). Various samples (characterized with different values of the AgNps and drug percentage added in distinct layers) with the same weight, thickness, and sterile time (40 min under UV light) were introduced into each well and incubated for 24, 48, and 72 h. Subsequently, cell viability was measured by the MTT assay with a microplate reader (Bio-Tec, ELX 800, and Winooski, VT). The control group consisted of the culture medium with pure cells, which were placed in the incubator for the same duration and under identical conditions as the samples. To eliminate random errors and enhance result accuracy, all experiments were conducted in triplicate [88].

Animal wound heal model

To investigate the effect of mupirocin and AgNps-loaded nanofibers on wound healing, 25 Wistar male rats, aged 6–8 weeks and weighing 200–250 gr, were anesthetized with an intraperitoneal injection of ketamine and xylazine in a volume ratio of 90/10. The experimental procedure was conducted in accordance with the policies and ethical principles at Kermanshah University of Medical Sciences. The dorsal surface of each mouse was disinfected with an alcohol swab and completely shaved. A burn injury was

induced by contact with a metal circular plate (thickness 0.3 cm and diameter 2.5 cm) heated to 95 °C and placed on the skin for 8 s [91, 92]. The rats were randomly divided into five experimental groups, and one hour after the burn injury, each animal received a nanofibrous mat of the same size as designed for their assigned group.

Group 1 consisted of injured rats treated with a PVA-Cs-Gel/PAN nanofibrous mat. Group 2 comprised injured rats treated with mupirocin-loaded nanofiber (PVA-Cs-Gel-Mu/PAN), and group 3 consisted of injured rats treated with both mupirocin and AgNps-loaded nanofiber (PVA-Cs-Gel-Mu/PAN-AgNps). Group 4 included injured rats treated solely with sterile gauze (negative control group), and Group 5 comprised injured rats treated with a typical commercial bandage dressing (Comfeel Plus) as a positive control. All groups underwent treatment for 28 days, and on the final day, a biopsy was performed on each group at the burn site.

Wound closure and healing rate

The wound area was measured at different time points, specifically on days 1, 7, 14, 21, and 28 after treatment. The wound closure (WC) is then calculated according to (Eq. 5) [91, 92]:

$$WC = \frac{A_i - A_t}{A_i} \times 100 \tag{5}$$

where A_i represents the initial wound area, and A_t refers to the wound area at different times after the treatment process.

Histopathological trial

At the end of the 28 days, samples, including skin adjacent to the wound, wound margin tissue, and the cutaneous wound, were soaked in 10% formalin for 48 h for paraffin exposure. Then, sections of the samples were stained using conventional hematoxylin–eosin and Masson's Trichrome Stain methods, and they were finally examined by light microscopy and a digital lens [11, 91, 92].

Statistical analysis

The data were analyzed as the mean standard error of the mean (SEM), which indicates how far the sample mean of the data is likely to be from the true population mean. Differences among the various groups of means were estimated using a one-way analysis of variance (ANOVA) with a Student's t test. Statistically significant differences were considered for values of $p \leq 0.05$.

Results and discussion

Investigation of the green AgNps

Morphological, physical, and chemical characterization results of the AgNps

The morphological and physicochemical characterization of the AgNps is presented
in Fig. 1. The result of the SEM analysis (Fig. 1a) revealed nearly spherical parti-
cles with an average diameter of 72.57 nm. Based on the dynamic light scattering
(DLS) results (Fig. 1d), the hydraulic diameter of the AgNps was approximately 211
nm, with a polydispersity index (PDI) of 0.376, falling within an acceptable range
(lower than 0.7). Due to the presence of surface hydration layers, DLS provides a
size measurement that is larger than the accurate size calculated by SEM [93]. Upon
comparing the FTIR spectra of the plant extract and the AgNps, as shown in Fig. 1b,
c, respectively, similar groups at about 3430, 2930, and 1640 cm^{-1} were identified,
corresponding to the stretching vibration of –OH, C–H, and C=O bonds [94].

The moderate and broad peak observed at the wavelength of 1062 cm^{-1} in the
plant extract (Fig. 1b), with a slight shift, could be detected at 1077 cm^{-1} in the
AgNps spectra (Fig. 1c) which may be attributed to C–O and OH vibration bonds
in organic acids. The minor peaks at 657.33, 622.76, and 526.9 cm^{-1} in the AgNps
were associated with the OH bonds in phenolic groups [95, 96]. Hydroxyl, phenolic,
and carbonyl in plant extract act as reducing agents for Ag ions. Also, the similarity
of these peaks could confirm the presence of absorbed components from the plant
extract on the surface of the AgNps, contributing to their enhanced stability. To ver-
ify this, a zeta potential analysis of the AgNps in water is shown in Fig. 1e, implying
a negative (− 12 mv) surface charge and a tendency toward particle repulsion. This
suggested the formation of a stable suspension [36, 60, 66, 67, 69, 93].

Since AgNps can absorb light in the range of 410–460 nm, the intensity of
UV–Vis absorption can be used as a criterion to determine the optimal concentra-
tion ratio of the plant extract to silver nitrate (1mM) [81]. As shown in Fig. 1f, the
volume ratios of plant extract to silver nitrate were (0.25/5), (0.5/5), (1/5), (2.5/5),
and (5/5), with corresponding intensities of 0.633, 0.774, 1.192, 0.446, and 0.438
nm, respectively. The optimal synthesis state was related to the concentration ratio
of 1/5, which exhibited the maximum adsorption light intensity at 446 nm. This
comparison suggested that an increase in the extract did not necessarily result in a
higher production of AgNps, indicating the presence of limiting agents in this reduc-
tion reaction.

Eventually, the X-ray analysis (Fig. 1g) displayed four main characteristic diffrac-
tion peaks at $2\theta = 38°$ (111), 44° (200), 64° (220), and 77.9° (311), indicative of the
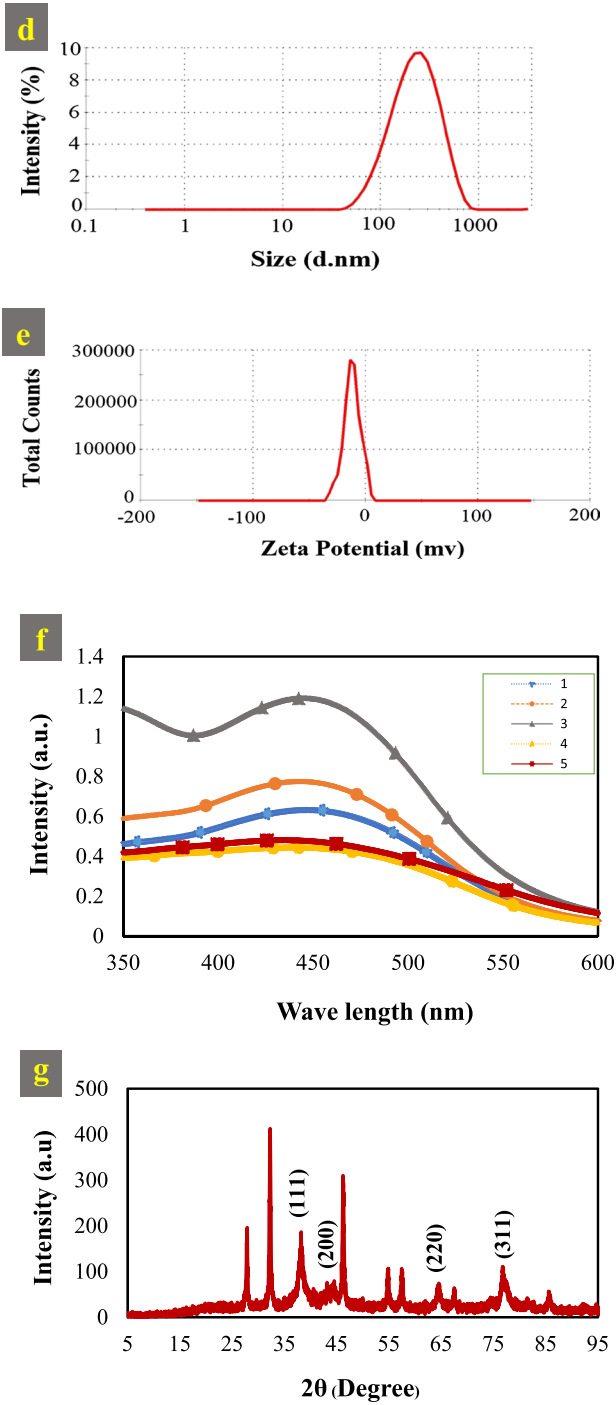cubic lattice of Ag [56, 57, 59, 60, 67–69, 81, 84, 96]. A closer examination of the
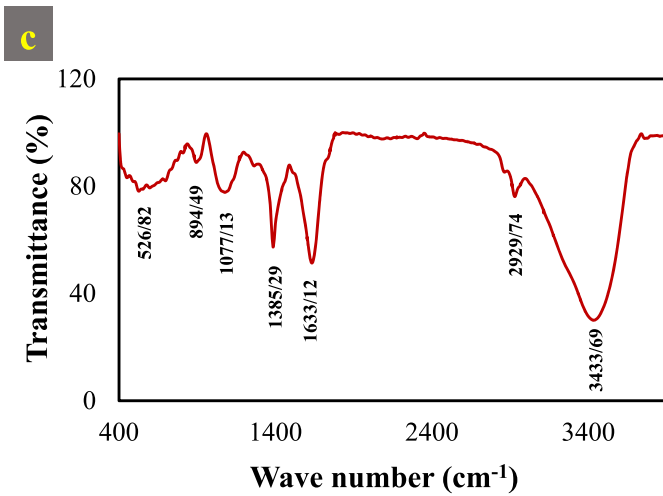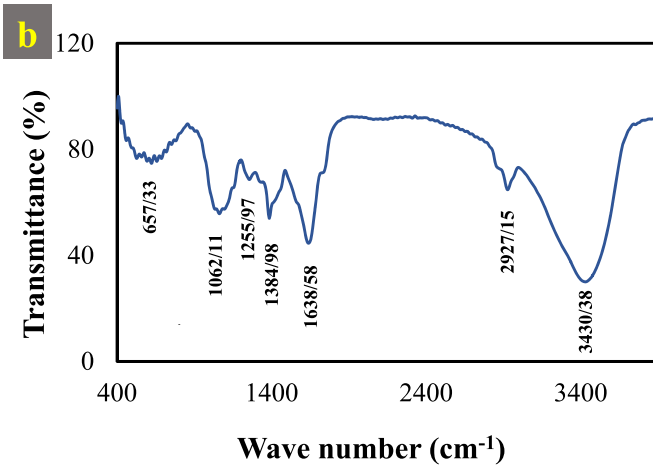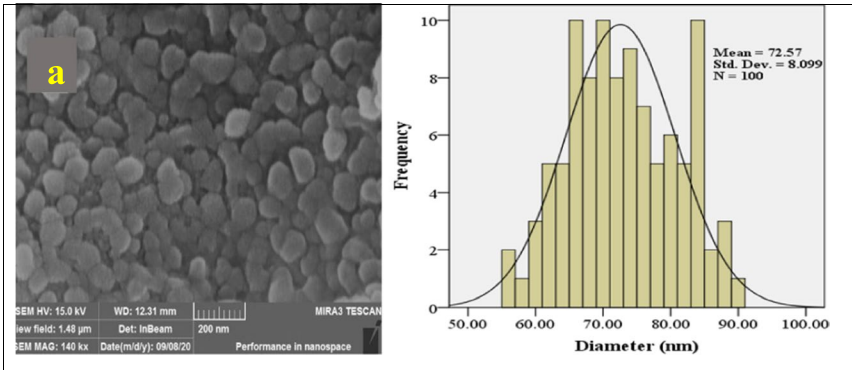
Fig. 1 (continued)

spectrum uncovered two additional peaks at $2\theta = 32°$ (202) and 46.17° (132), which matched with standard JCPDS data (JCPDS, NO 84-1108). Low-intensity peaks observed for AgO indicated that the samples predominantly consisted of the AgNps with a small amount of AgO (either incorporated or as a layer on the surface of the AgNps).

Antibacterial activity of the AgNps

Despite the extensive use of AgNps as an antibacterial agent, the mechanism of their effect on microorganisms is not fully understood [57]. The growth of gram-positive *Staphylococcus aureus* (PTTC1431) and gram-negative *Escherichia coli* (PTCC1522) was examined in the presence and absence of the AgNps, and the quantitative results are depicted in Fig. 2. According to these results, the inhibition of the growth of gram-negative bacteria was more effective than that of gram-positive bacteria. This difference could be attributed to the diffusion of ions from the surface of the AgNps and their binding to cell membranes. This finding supported the theory that the lipopolysaccharide proteins in the wall are associated with the different functions of bacterial cells, and the binding of the AgNps to these proteins could be a major factor in reducing bacterial activity. On the other hand, the cell membrane of gram-positive bacteria is thicker than gram-negative bacteria, which could impede the penetrating of AgNps into the bacterial cytoplasm, ultimately leading to higher levels of the MIC and MBC in *S. aureus* bacteria [59, 61, 68, 81, 97–99].

Morphological investigation of nanofibers

Nanofiber morphology and diameter size distribution of electrospun samples at 20 µm scale are shown in Fig. 3. Under optimal electrospinning conditions, each bilayer generated smooth, uniform, and relatively knot-free nanofibers. In
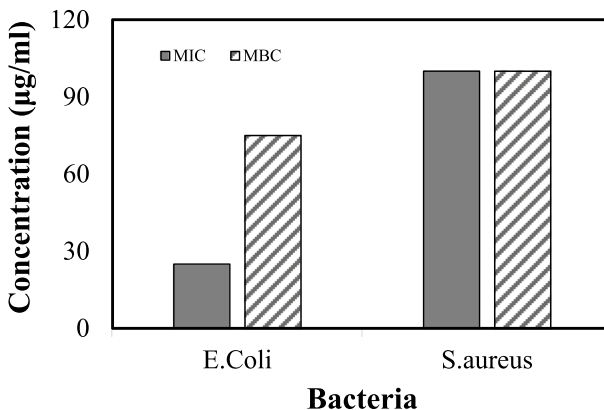
Fig. 2 Minimum inhibitory and minimum bactericidal concentrations of the AgNps against *E. coli* and *S. aureus* bacteria
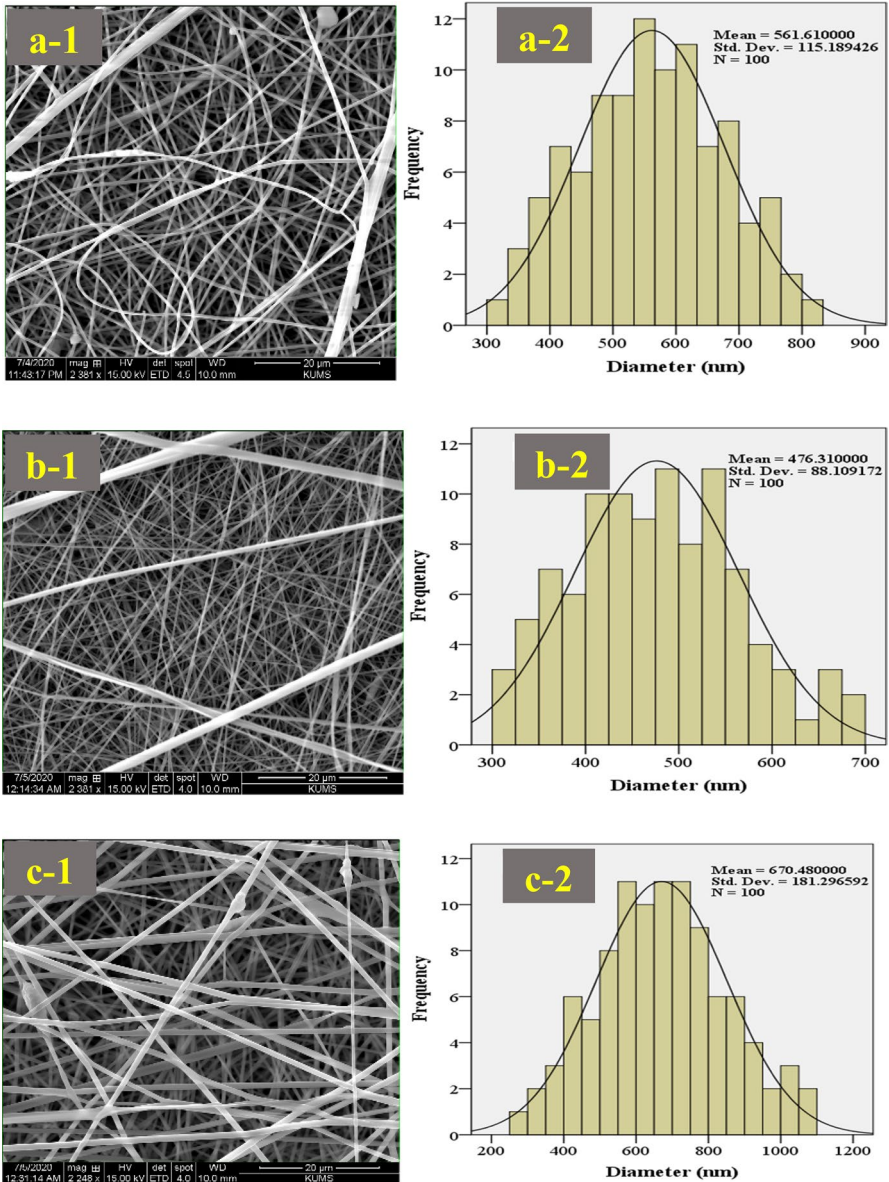
Fig. 3 SEM micrographs of nanofibers, **a-1** PVA-CS-Gel/PAN; **a-2** respective size analyzing results, **b-1** PVA-CS-Gel + 3 wt% Mu/PAN; **b-2** respective size analyzing results, **c-1** PVA-CS-Gel + 3 wt% Mu/PAN + 1 wt% AgNps; **c-2** respective size analyzing results, **d-1** PVA-CS-Gel + 3 wt% Mu + 0.5 wt% AgNps/PAN + 1 wt% AgNps; **d-2** respective size analyzing results, and **e-1** PVA-CS-Gel + 3 wt% Mu + 1 wt% AgNps/PAN + 1 wt% AgNps; **e-2** respective size analyzing results
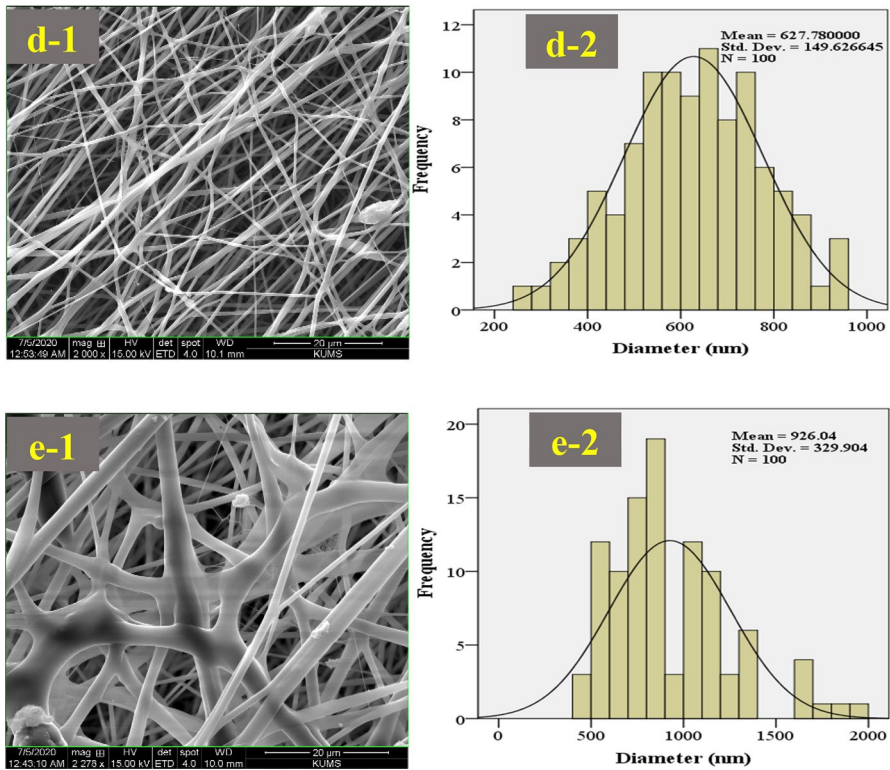
Fig. 3 (continued)

the polymer state (Fig. 3a-1), these nanofibers exhibited a diameter of only 561.6 nm (Fig. 3a-2). The addition of mupirocin to the polymer solution of the lower layer (the layer in direct contact with the skin) reduced the viscosity, leading to a diminished fiber diameter of 476.31 nm, as depicted in Fig. 3b-1 and b-2 [10].

Upon introducing AgNps to the polymer solution, both viscosity and electrical conductivity increase. The elevated viscosity results in an increase in fiber diameter, while the heightened electrical conductivity induces a reduction in nanofiber diameter [100, 101]. Analysis of the nanofiber diameter measurements in Fig. 3c-1 and 3d-1 revealed that addition of the AgNps at a concentration of 1 wt% to the top layer solution significantly boosted viscosity, causing a substantial rise in nanofiber diameter to 670.5 nm (Fig. 3c-2).

However, the introduction of 0.5 wt% of the AgNps to the bottom layer, accompanied by a simultaneous increase in viscosity, led to a reduction in nanofiber diameter to 627.78 nm (Fig. 3d-2). Hence, it can be deduced that at different AgNps concentrations, the predominant influence on nanofiber diameter was determined by the prevailing impact of either viscosity or electrical conductivity within the solution. Figure 3e-1 illustrates the structure of nanofibers derived from a solution containing 1 wt% of the AgNps in the bottom layer.

Despite possessing an average diameter of 924.04 nm (Fig. 3e-2), these nanofibers exhibited a lack of proper and uniform diameter distribution. Observations during the electrospinning process indicated an excessively high viscosity in this specific solution, resulting in complications such as regular nozzle clogging. This issue was significantly alleviated by reducing the AgNps concentration to 0.5 wt%, thereby effectively streamlining the electrospinning process. SEM images, combined with the results of the viscometry test and morphological studies, provided further support and validation for these findings.
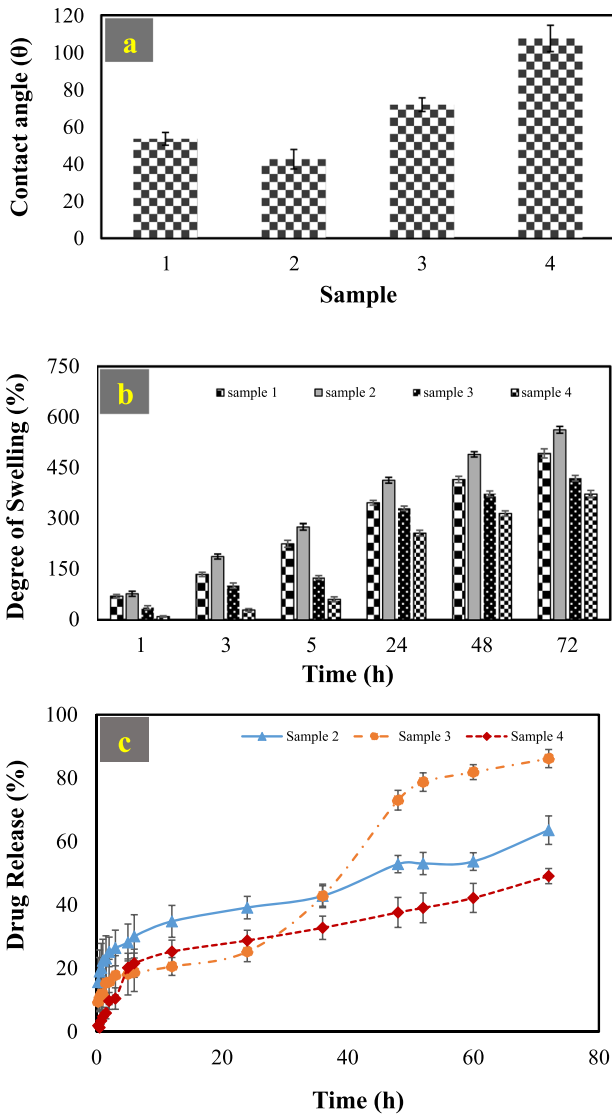
Water contact angle, swelling and drug release of nanofibers

Figure 4a presents the results of the contact angle analysis using water droplets on electrospun samples. Evidently, the addition of the drug to the bottom layer in sample 2 (PVA-Cs-Gel + 3 wt% Mu/PAN) amplified the hydrophilicity of nanofibers due to the drug's relatively hydrophilic nature. Therefore, the contact angle decreased from 51.63 in sample 1 (PVA-CS-Gel/PAN) to 42.614 degrees. In Sample 3 (PVA-Cs-Gel + 3 wt% Mu/PAN + 1 wt% AgNps), the hydrophobicity of the AgNps led to an increased contact angle of 84.71 degrees. For sample 4 (PVA-Cs-Gel + 3 wt% Mu + 0.5 wt% AgNps/PAN + 1 wt% AgNps), adding the AgNps to the bottom layer reduced its hydrophilicity, resulting in an elevated contact angle of 107 degrees. Notably, a contact angle between 60 and 80 degrees enhances the potential for cell adhesion capacity, a phenomenon observed in samples 1 to 3 [36, 102].

The swelling test is another criterion parameter that significantly impacts both the drug release rate and wound healing. An optimal swelling rate is pivotal for ensuring proper adherence of the wound and facilitating damage-free removal [10, 103]. Figure 4b illustrates the swelling outcomes of the samples over durations of 1, 3, 5, 24, 48, and 72 h. The results indicated a decrease in nanofiber swelling with an increase in the concentration of the AgNps. This reduction could be attributed to fewer free spaces originated from the presence of the AgNps, along with a reduced hydrophilicity. In addition, the inclusion of the AgNps in the polymer matrix created a tortuous path, hindering the passage of water molecules. Moreover, observation revealed that during initial hours, all samples exhibited a higher rate of inflation owing to increased water absorption. However, with time, as fiber degradation occurred, the swelling rate increased at a lower slope. The contact angle test results, indicating the maximum and minimum hydrophilicity for samples 2 and 4, respectively, were corroborated by confirmed by the swelling test findings. Given the sample 1 served as a drug-free polymer substrate, release diagrams were scrutinized for the remaining three samples. A comprehensive examination of the release diagram (Fig. 4c) for samples 2, 3, and 4 unveiled three distinct phases.

The first stage was characterized by burst release, where Mu underwent rapid release through the dissolution of the fibers and the leaching of surface drugs from the nanofiber's pores [8, 31, 93]. In the subsequent stage, the drug release mechanism was primarily based on penetration. In this phase, due to the partial washout of the drug in the first stage, the unreleased drugs passed through the pores at a low and nearly constant speed. Finally, the third stage involved the

Fig. 4 SEM micrographs of nanofibers **a** Water contact angle; **b** Degree of swelling (%); **c** The results of the release profile of mupirocin into PBS from bilayer nanofibers, sample (1) PVA-Cs-Gel/PAN, sample (2) PVA-Cs-Gel+3 wt% Mu/PAN, sample (3) PVA-Cs-Gel+3 wt% Mu/PAN+1%wt AgNps, and sample (4) PVA-Cs-Gel+3 wt% Mu+0.5% wt AgNps/PAN+1%wt AgNps

release of drugs trapped in the polymer matrix. During this step, deeply embedded drugs were released due to polymer degradation, bond breakage, and monomer production. They entered the release medium alongside the buffer flow, leading to a sudden increase in the drug release rate [104].

In a closer examination of sample 2, which demonstrated the lowest contact angle in the absence of AgNps (Fig. 4a) and a higher swelling rate at various times compared to the other two samples (Fig. 4b), a release of approximately 20% in the first hour, 41% in the subsequent 36 h, and ultimately 63% after 72 h could be justified. The correlation between the release behavior and the swelling diagram suggested that the primary factor governing controlled release in this sample was the gradual degradation of the polymer matrix and the infiltration of the drug into the buffer medium. The results of the kinetic study of drug release from polymeric substrates using the Korsmeyer-Peppas model are presented in Table 1. According to this model, the release exponent was 0.216, indicating a release mechanism consistent with physical penetration. Table 1 displays that the Higuchi model yielded the best regression coefficient, equal to $R^2 = 0.9772$.

In sample 3, the release attained 10% in the initial hour and reached 17% within the first 3 h. Subsequently, during the second stage, with a gradual incline over 28 h, the release rate reached 27%. The third stage of release extended up to 52 h, during which the drug release rate escalated to 78%, ultimately reaching 86% after 72 h. The release mechanism was identified as Fickian diffusion ($n = 0.377$), aligning well with first-degree and zero-degree models. These models are particularly suitable for elucidating the release behavior of highly soluble drugs, such as Mu from porous skin patches.

In sample 4, where the AgNps were present in both layers, the contact angle exhibited a significant increase, reaching 107.529 degrees, aligning with the swelling results observed at different times. The initial release was approximately 1.8%, escalating to 20% after 5 h, representing a lower burst release compared to the other two samples. The distinct release pattern of sample 3, as discussed in the previous section regarding its swelling behavior, warranted closer examination. Despite having lower swelling and hydrophilicity than sample 2, sample 3 exhibited a higher release rate in the third stage. This difference may be attributed to the release of the loaded AgNps from the nanofiber and the presence of these ions in the environment, gradually increasing the ionic strength and pH of the medium.

These two factors mutually influence the release of the drug, where an increase in pH enhances the drug release [105], while an increase in ionic strength diminishes it [106]. Consequently, it can be inferred that in sample 3, the presence and release of silver, coupled with a moderate increase in pH, resulted in an increased drug release after approximately 28 h. Conversely, in sample 4, where silver was

Table 1 Results of the kinetic study

Sample No	Regression of different models			Release exponent	Drug release mechanism
	Zero-order	First-order	Higuchi		
2	0.9672	0.9158	0.9772	0.216	Fick diffusion
3	0.9435	0.9457	0.8590	0.377	Fick diffusion
4	0.8744	0.5485	0.9556	0.908	Non-Fick diffusion
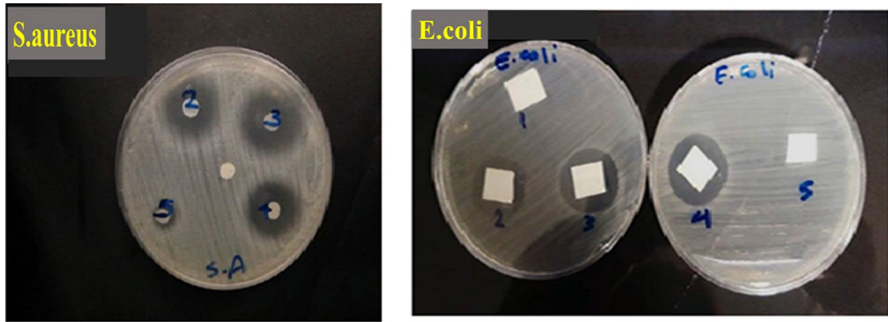
Fig. 5 Results of the antibacterial assay of nanofibers exposed to gram-positive *S. aureus* and gram-negative *E. coli*, sample (1) PVA-Cs-Gel/PAN, sample (2) PVA-Cs-Gel + 3 wt% Mu/PAN, sample (3) PVA-Cs-Gel + 3 wt% Mu/PAN + 1 wt% AgNps, sample (4) PVA-Cs-Gel + 3 wt% Mu + 0.5 wt% AgNp/PAN + 1 wt % AgNps, and sample (5) PVA-Cs-Gel + 3 wt % Mu + 1 wt% AgNp/PAN + 1 wt% AgNps

Table 2 Evaluation of inhabitation zone of nanofiber against gram-positive *S. aureus* and gram-negative *E. coli*	Sample	Diameter of inhabitation zone (mm)	
		E. coli	*S. aureus*
	1	0	0
	2	16.4	21.6
	3	17.2	28
	4	18.7	23
	5	0	8.9

present in both layers, the dominant effect of ionic strength might lead to a lower drug release rate compared to the other two samples after the initial rapid release.

Antibacterial activity of nanofibers

Burn injuries are particularly vulnerable to infection caused by both gram-positive bacteria such as *S. aureus* and gram-negative bacteria such as *E. coli*. The antibacterial properties of the nanofibrous mats were evaluated using the disk diffusion method, assessing the bacterial growth inhibition zone around five samples: sample 1 as a control (PVA-CS-Gel /PAN), sample 2 (PVA-CS-Gel + 3 wt% Mu/PAN), sample 3 (PVA-CS-Gel + 3 wt% Mu/PAN + 1 wt% AgNps), sample 4 (PVA-CS-Gel + 3 wt% Mu + 0.5 wt% AgNps/PAN + 1 wt% AgNps), and sample 5 (PVA-CS-Gel + 3 wt% Mu + 1 wt% AgNp/PAN + 1 wt% AgNps). Qualitative and quantitative results are shown in Fig. 5 and Table 2, respectively. This type of nanoparticle readily adheres to cell membranes, destabilizing the plasma potential and subsequently penetrating the respiratory chain. By halting cellular respiration within the mitochondrial membrane, it leads to complete microbial death.

Additionally, silver ions react with the thiol groups of crucial bacterial enzymes, rendering them inactive. This inactivation disrupts the bacterial DNA's ability to

multiply under these conditions [97, 98, 107]. Therefore, the greater the quantity of AgNps loaded into the nanofibers, the more extensive the zone of non-growth, and consequently, the stronger the antibacterial property. As illustrated in Fig. 5, sample 4, featuring the highest nanoparticle content, exhibited the largest non-growth zone, while sample 2, lacking nanoparticles, displayed the smallest halo. Indeed, in samples 3 and 4, due to the synergistic effect of the AgNps and Mu, the antibacterial property of the nanofiber was boosted. In sample 5, where the AgNps were added up to 1 wt% by weight near the drug, the excessive viscosity of the solution hindered proper electrospinning, impeding the effective release of the AgNps from the nanofiber. Consequently, its antibacterial properties against *E. coli* were not manifested due to inadequate release.

In the case of *S. aureus* bacteria, it was observed that sample 2 exhibited a smaller non-growth halo compared to samples 3 and 4. Despite having the highest drug release within the first 24 h, sample 2, lacking AgNps, demonstrated the least antibacterial effect. The addition of the AgNps to the upper layer (the layer in contact with the environment) led to a reduction in drug release during the initial 24 h. However, due to the antibacterial properties of AgNps, the reported halo was greater than that of sample 2. Furthermore, incorporating the AgNps into the lower layer (the layer in contact with the skin) near the Mu resulted in a slower drug release than sample 3, leading to a smaller halo compared to sample 3. Notably, despite the smaller halo, this sample exhibited stronger antibacterial properties than sample 2, similar to sample 3. Regarding sample 5, as mentioned earlier, the dampness of the fibers resulted in only a small amount of Mu being deposited on the fiber, causing a minimal halo for *S. aureus* bacteria.

MTT cytotoxicity of nanofibers

When applying an ideal wound dressing, it should not release toxic substances that could induce wound inflammation and cell death. Therefore, samples underwent testing using the 3-(4, 5-Dimethylthiazol-2-yl)-2, 5-Diphenyltetrazolium Bromide
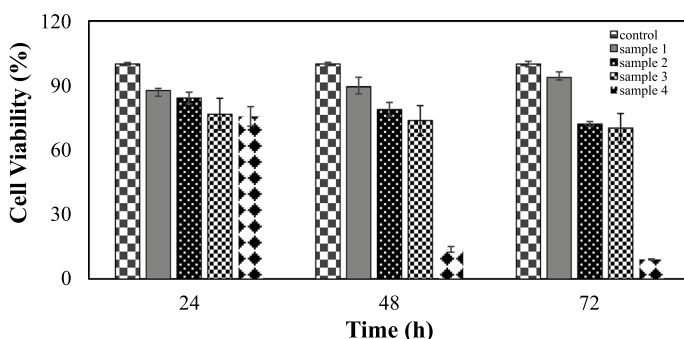
Fig. 6 Results of the cytotoxicity evaluation of nanofibers, control) fibroblast cell without nanofiber, sample (1) PVA-Cs-Gel/PAN, sample (2) PVA-Cs-Gel + 3 wt% Mu/PAN, sample (3) PVA-Cs-Gel + 3 wt% Mu/PAN + 1 wt% AgNps, sample (4) PVA-Cs-Gel + 3 wt% Mu + 0.5 wt% AgNp/PAN + 1 wt% AgNps, and sample (5) PVA-Cs-Gel + 3 wt % Mu + 1 wt% AgNp/PAN + 1 wt% AgNps

(MTT) cytotoxicity analysis to identify the most suitable sample for animal studies. The results of this test are depicted in Fig. 6. Fibroblasts without nanofibers were considered as the control group. In sample 1 not only was there no toxicity observed, but also an increase in growth was detected over time. The primary reason could be attributed to the degradation of fibers, leading to the release of gelatin and chitosan polymers. These polymers served as nutrients by the cells and promoted cell growth [34, 108]. In sample 2, containing the drug, the cell viability percentage exhibited a downward trend over time (24, 48, and 72 h), correlating with the increased release of the drug and indicating Mu-induced toxicity.

Moreover, the survival rate of fibroblast cells exceeded the IC50 (lethal concentration for half of the cells) [11], making it an acceptable level of toxicity. In sample 3, where the AgNps were added to the top layer, as expected, the cell viability percentage decreased due to the toxicity caused by the AgNps, compared to sample 2. However, as demonstrated, the placement of the AgNps in the top layer, which was not in direct contact with the culture medium, resulted in limited toxicity and survival rate of fibroblast cells remained higher than the IC50. In other words, there is a meaningful connection between surface charge of the Nps and their penetration depth. The more negative the zeta potential, the lower the penetration depth. Actually, the strong electrostatic repulsion between the Nps and the skin with a negative surface charge considerably impedes penetration into the deep layers of the skin [3, 109].

High doses of AgNps are toxic substances that can damage the mitochondria of the cells, disrupt the cellular respiration process, and eventually cause cell death. In sample 4, due to the presence of the AgNps in the vicinity of the drug and direct contact with the skin, it had a more profound penetrating effect on skin cells. In the first 24 h, drug and the AgNps release rates were lower, and the percentage of lethality was slightly decreased. However, over time, specifically 48 and 72 h after release, the deadly effect of the cell intensified, resulting in a lower survival rate of fibroblast cells than IC50 within 72 h. Therefore, it was concluded that placing this quantity of the AgNps in contact with the skin was not a prudent choice, and sample 3, with its higher biocompatibility, was more suitable for use as a wound dressing in subsequent animal studies.

Wound healing and its closure

Figure 7 displays the wound healing process in animal samples coated with different groups. The macroscopic images of the wound healing process at different times, specially 1, 7, 14, 21, and 28 days can be observed in Fig. 7A. Additionally, the precise percentage of the wound closures is plotted in Fig. 7B. The results of examining the healing process in burn wounds showed that in the negative control group, a gas bandage adhered to the wound surface, causing damage to newly regenerated tissues.

Wounds covered with Comfeel Plus dressing (positive control) exhibited superior performance compared to the negative control group. This dressing demonstrated a higher water absorption capacity, maintaining a moist wound environment [110].
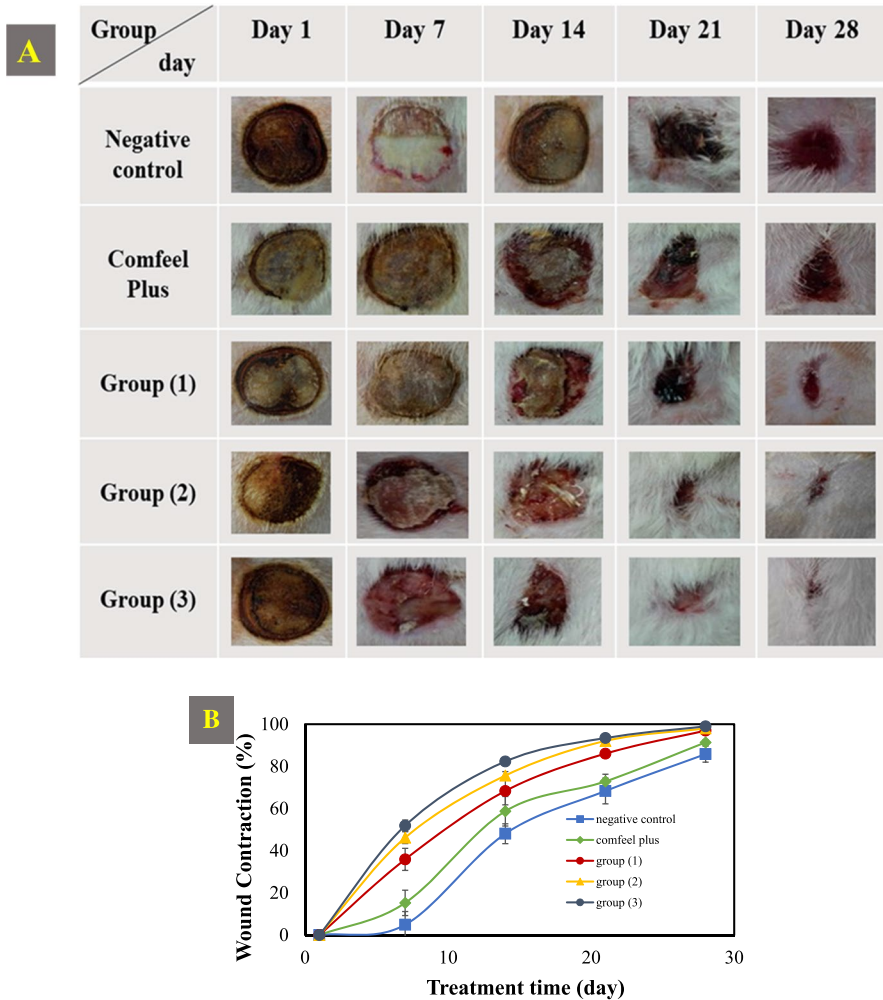
Fig. 7 Results of the image analysis of the burn wound healing steps in animal samples coated with different groups (**A**); and wound closure rate (**B**) in different time period of 1, 7, 14, 21 and 28 days, group1) PVA-Cs-Gel/PAN, group2) PVA-Cs-Gel + 3 wt% Mu/PAN, group3) PVA-Cs-Gel + 3 wt% Mu/PAN + 1 wt% AgNps

Epithelial cells migration through the surface of the damaged tissues is influenced by the type of wound surface, impacting the speed of this migration. Wet wound surfaces accelerate this process, promoting the growth and formation of fibroblast cells, whereas dry surfaces act as a barrier [111]. Therefore, one of the main objectives of wound dressing is to sustain adequate moisture levels and expedite the regeneration of epithelial tissue [112].

The nanofiber dressings used in groups 1, 2, and 3 showed higher water absorption capacity because of their elevated surface area-to-volume ratio [38] and the hydrophilic nature of the polymers used in the first layer (PVA, CS, and Gel). As

a result, similar to the Comfeel Plus group, they outperformed the negative control group. In addition, these nanofibers, owing to their nanostructure, indicated excellent water vapor and oxygen passage. This characteristic contributed to the surpassing performance of these three groups compared to the Comfeel Plus group, as Comfeel dressing lacks optimal permeability.

Histopathological examination

In Fig. 8, histopathological images of the skin are presented. From Fig. 8 (up), it could be inferred that healthy skin exhibited a thick wall, comprising the epidermis
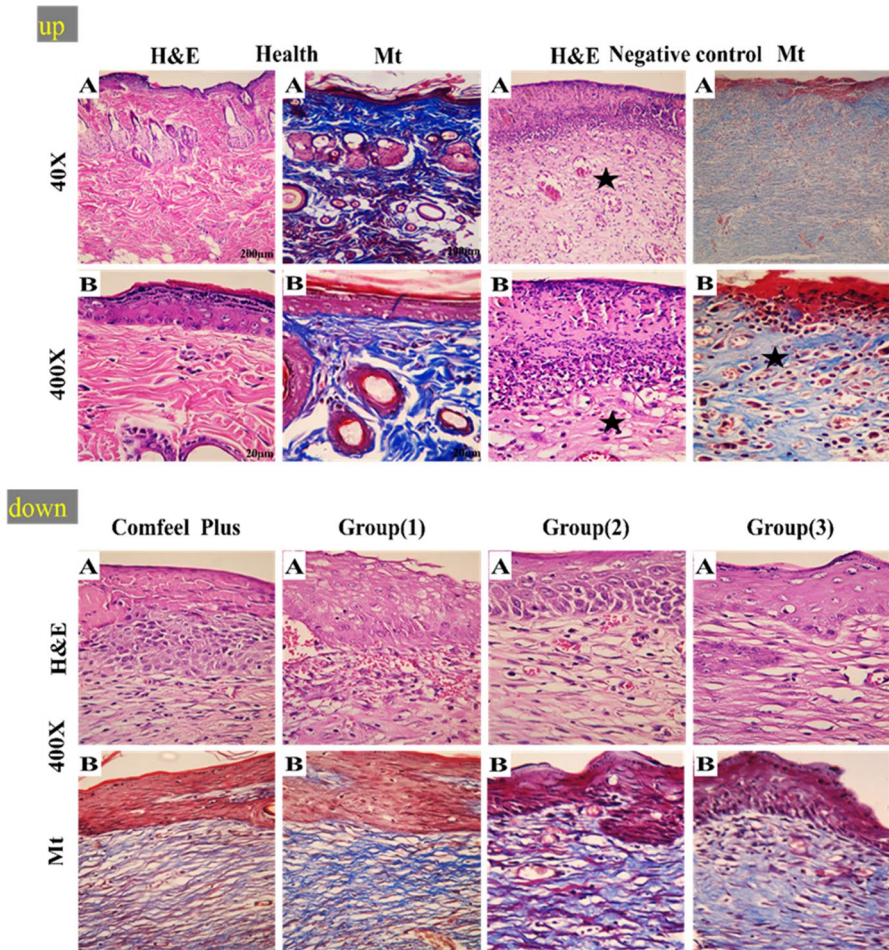
Fig. 8 Results of the histopathological imaging of healthy skin and burn wounds bandaged with negative control) gauze (up); Comfeel Plus, group (1) PVA-Cs-Gel/PAN, group (2) PVA-Cs-Gel + 3 wt% Mu/PAN, group (3) PVA-Cs-Gel + 3 wt% Mu/PAN + 1 wt% AgNps (down) using **A** hematoxylin–eosin (H&E), and **B** Trichrome Masson (Mt) staining after 28 days

and dermal connective tissue containing dermal appendages, various cells, and densely formed connective fibers (blue). In gas-treated skin wounds (negative control), a disorganized tissue structure was observed. In the superficial part of the wound, necrotic tissue was formed, and inflammatory phase cells were present under the necrotic tissue. Furthermore, in the extracellular matrix, collagen fibers were sparse and irregular, marked with an asterisk.

According to the images in Fig. 8 (down), the Comfeel Plus treatment group demonstrated lower levels of necrotic tissue and inflammatory cell accumulations compared to the negative control group, with denser collagen fibers. In mice treated with group 1, skin injuries were reduced in comparison with both the negative and positive control groups. For the bandaged samples in group 2 and group 3, skin tissue repair extended to a broader extent compared to the other mentioned treatment groups. Moreover, the cells and connective fibers appeared normal.

Conclusion

Electrospun materials have been thoroughly investigated for various medical applications, particularly in the field of wound dressing. Nevertheless, the creation of an optimal environment for protecting wounds against external infections and the repair of damaged cells without toxic reactions or irritation to the skin remain significant challenges. For this purpose, bilayer nanofiber (PVA-CS-Gel/PAN) was successfully developed using the electrospinning technique. These dressings contain varying percentages of mupirocin and *Capsella bursa-pastoris*-AgNps, exhibiting multifunctional properties such as excellent absorbing capacity, cytocompatibility, and antibacterial properties. While green-synthesized AgNps exhibit high antibacterial properties, the distribution of these nanoparticles within the body may lead to potential negative consequences or harmful effects. To address this concern, the AgNps were loaded into the top layer to prevent the invasion of environmental microbes to the wound site, serving a protective role. It is important to note that achieving the highest antibacterial activity must be balanced with maintaining levels of AgNps that are compatible with skin fibroblast cells. Based on the obtained results, a scaffold containing 3 wt% Mu in the bottom layer and 1 wt% AgNps in the top layer demonstrated a synergistic effect between the controlled release drug and the AgNps at the optimum concentration, ensuring the effective performance of the nanofiber against both gram-positive and gram-negative bacteria, along with acceptable cell compatibility. Additionally, the scaffold exhibited acceptable outcomes in terms of swelling and contact angle, contributing to the reduction in wound infection and efficient collection of secretions. Ultimately, the analysis of both macroscopic images and histological studies revealed that in comparison with the other groups, these nanofibers exhibited favorable effects on wound closure and healing through appropriate processes of re-epithelialization and collagen deposition in the injured rat skin. Consequently, these therapeutic effects make the developed nano-bandage well-suited for healthcare applications, including wound dressings.

Declarations

Conflict of interest The authors declare no conflict of interest in this work.

References

1. Behere I, Ingavle G (2022) In vitro and in vivo advancement of multifunctional electrospun nanofiber scaffolds in wound healing applications: innovative nanofiber designs, stem cell approaches, and future perspectives. J Biomed Mater Res Part A 110(2):443–461
2. Albertia T, Coelhoa DS, Voytenaa A, Pitza H, de Práa M, Mazzarinoa L, Kuhnenb S, Ribeiro-do-Vallea RM, Maraschina M, Veleirinho B (2017) Nanotechnology: a promising tool towards wound healing. Curr Pharm Des 23:1–14
3. Liang XW, Xu ZP, Grice J, Zvyagin AV, Roberts MS, Liu X (2013) Penetration of nanoparticles into human skin. Curr Pharm Des 19(35):6353–6366
4. Hajilou H, Farahpour MR, Hamishehkar H (2020) Polycaprolactone nanofiber coated with chitosan and Gamma oryzanol functionalized as a novel wound dressing for healing infected wounds. Int J Biol Macromol 164:2358–2369
5. Balaji A, Jaganathan SK, Ismail AF, Rajasekar R (2016) Fabrication and hemocompatibility assessment of novel polyurethane-based bio-nanofibrous dressing loaded with honey and *Carica papaya* extract for the management of burn injuries. Int J Nanomed 11:4339
6. Saghazadeh S, Rinoldi C, Schot M, Kashaf SS, Sharifi F, Jalilian E, Nuutila K, Giatsidis G, Mostafalu P, Derakhshandeh H (2018) Drug delivery systems and materials for wound healing applications. Adv Drug Deliv Rev 127:138–166
7. Alinezhad Sardareh E, Shahzeidi M, Salmanifard Ardestani MT, Mousavi-Khattat M, Zarepour A, Zarrabi A (2022) Antimicrobial activity of blow spun PLA/gelatin nanofibers containing green synthesized silver nanoparticles against wound infection-causing bacteria. Bioengineering 9(10):518
8. Eming SA, Martin P, Tomic-Canic M (2014) Wound repair and regeneration: mechanisms, signaling, and translation. Sci Transl Med 6(265):265sr6-265sr6
9. Jeckson TA, Neo YP, Sisinthy SP, Gorain B (2021) Delivery of therapeutics from layer-by-layer electrospun nanofiber matrix for wound healing: an update. J Pharm Sci 110(2):635–653
10. Xia D, Liu Y, Cao W, Gao J, Wang D, Lin M, Liang C, Li N, Xu R (2022) Dual-functional nanofibrous patches for accelerating wound healing. Int J Mol Sci 23(18):10983
11. Gao Z, Su C, Wang C, Zhang Y, Wang C, Yan H, Hou G (2021) Antibacterial and hemostatic bilayered electrospun nanofibrous wound dressings based on quaternized silicone and quaternized chitosan for wound healing. Eur Polym J 159:110733
12. Dwivedi C, Pandey H, Pandey AC, Ramteke PW (2016) Nanofibre based smart pharmaceutical scaffolds for wound repair and regenerations. Curr Pharm Des 22(11):1460–1471
13. Baukum J, Pranjan J, Kaolaor A, Chuysinuan P, Suwantong O, Supaphol P (2020) The potential use of cross-linked alginate/gelatin hydrogels containing silver nanoparticles for wound dressing applications. Polym Bull 77:2679–2695
14. Osanloo M, Arish J, Sereshti H (2020) Developed methods for the preparation of electrospun nanofibers containing plant-derived oil or essential oil: a systematic review. Polym Bull 77:6085–6104
15. Zhang X, Wang Y, Gao Z, Mao X, Cheng J, Huang L, Tang J (2023) Advances in wound dressing based on electrospinning nanofibers. J Appl Polym Sci 4:e54746

16. Lukomskyj AO, Rao N, Yan L, Pye JS, Li H, Wang B, Li JJ (2022) Stem cell-based tissue engineering for the treatment of burn wounds: a systematic review of preclinical studies. Stem Cell Rev Rep 18:1–30

17. Bozkaya O, Arat E, Gök ZG, Yiğitoğlu M, Vargel I (2022) Production and characterization of hybrid nanofiber wound dressing containing *Centella asiatica* coated silver nanoparticles by mutual electrospinning method. Eur Polym J 166:111023

18. Chen P, Chai M, Mai Z, Liao M, Xie X, Lu Z, Zhang W, Zhao H, Dong X, Fu X (2022) Electrospinning polyacrylonitrile (PAN) based nanofiberous membranes synergic with plant antibacterial agent and silver nanoparticles (AgNPs) for potential wound dressing. Mater Today Commun 31:103336

19. Daglar O, Altinkok C, Acik G, Durmaz H (2020) Electrospinning of poly(1,4-cyclohexanedimethylene acetylene dicarboxylate): study on the morphology, wettability, thermal and biodegradation behaviors. Macromol Chem Phys 221(23):2000310

20. Croitoru A-M, Ficai D, Ficai A, Mihailescu N, Andronescu E, Turculet SC (2020) Nanostructured fibers containing natural or synthetic bioactive compounds in wound dressing applications. Materials 13(10):2407

21. Dias J, Granja P, Bártolo P (2016) Advances in electrospun skin substitutes. Prog Mater Sci 84:314–334

22. Su S, Bedir T, Kalkandelen C, Başar AO, Şaşmazel HT, Ustundag CB, Sengor M, Gunduz O (2021) Coaxial and emulsion electrospinning of extracted hyaluronic acid and keratin based nanofibers for wound healing applications. Eur Polym J 142:110158

23. Torres-Martínez EJ, Cornejo Bravo JM, Serrano Medina A, Pérez González GL, Villarreal Gómez LJ (2018) A summary of electrospun nanofibers as drug delivery system: drugs loaded and biopolymers used as matrices. Curr Drug Deliv 15(10):1360–1374

24. Afsharian YP, Rahimnejad M (2021) Bioactive electrospun scaffolds for wound healing applications: a comprehensive review. Polym Test 93:106952

25. Guo Z, Poot AA, Grijpma DW (2021) Advanced polymer-based composites and structures for biomedical applications. Eur Polym J 149:110388

26. Dias J, Baptista-Silva S, De Oliveira C, Sousa A, Oliveira AL, Bártolo P, Granja P (2017) In situ crosslinked electrospun gelatin nanofibers for skin regeneration. Eur Polym J 95:161–173

27. Yang S, Li X, Liu P, Zhang M, Wang C, Zhang B (2020) Multifunctional chitosan/polycaprolactone nanofiber scaffolds with varied dual-drug release for wound-healing applications. ACS Biomater Sci Eng 6(8):4666–4676

28. Abrigo M, McArthur SL, Kingshott P (2014) Electrospun nanofibers as dressings for chronic wound care: advances, challenges, and future prospects. Macromol Biosci 14(6):772–792

29. Adeli H, Khorasani MT, Parvazinia M (2019) Wound dressing based on electrospun PVA/chitosan/starch nanofibrous mats: fabrication, antibacterial and cytocompatibility evaluation and in vitro healing assay. Int J Biol Macromol 122:238–254

30. Keshvardoostchokami M, Majidi SS, Huo P, Ramachandran R, Chen M, Liu B (2020) Electrospun nanofibers of natural and synthetic polymers as artificial extracellular matrix for tissue engineering. Nanomaterials 11(1):21

31. Lett JA, Sagadevan S, Fatimah I, Hoque ME, Lokanathan Y, Léonard E, Alshahateet SF, Schirhagl R, Oh WC (2021) Recent advances in natural polymer-based hydroxyapatite scaffolds: properties and applications. Eur Polym J 148:110360

32. Tran T, Hamid Z, Cheong K (2018) A review of mechanical properties of scaffold in tissue engineering: *Aloe vera* composites. In: Journal of physics: conference series. IOP Publishing

33. Tan G, Wang L, Pan W, Chen K (2022) Polysaccharide electrospun nanofibers for wound healing applications. Int J Nanomed 28:3913–3931

34. Bano I, Arshad M, Yasin T, Ghauri MA, Younus M (2017) Chitosan: a potential biopolymer for wound management. Int J Biol Macromol 102:380–383

35. Cui C, Sun S, Wu S, Chen S, Ma J, Zhou F (2021) Electrospun chitosan nanofibers for wound healing application. Eng Regen 2:82–90

36. Kalantari K, Mostafavi E, Saleh B, Soltantabar P, Webster TJ (2020) Chitosan/PVA hydrogels incorporated with green synthesized cerium oxide nanoparticles for wound healing applications. Eur Polym J 134:109853

37. Das A, Ringu T, Ghosh S, Pramanik N (2022) A comprehensive review on recent advances in preparation, physicochemical characterization, and bioengineering applications of biopolymers. Polym Bull 80:1–66

38. Ulubayram K, Calamak S, Shahbazi R, Eroglu I (2015) Nanofibers based antibacterial drug design, delivery and applications. Curr Pharm Des 21(15):1930–1943
39. Li H, Chen X, Lu W, Wang J, Xu Y, Guo Y (2021) Application of electrospinning in antibacterial field. Nanomaterials 11(7):1822
40. Bacakova L, Zikmundova M, Pajorova J, Broz A, Filova E, Blanquer A, Matejka R, Stepanovska J, Mikes P, Jencova V (2019) Nanofibrous scaffolds for skin tissue engineering and wound healing based on synthetic polymers. Appl Nanobiotechnol 8:1
41. Coelho DS, Veleirinho B, Alberti T, Maestri A, Yunes R, Dias PF, Maraschin M (2018) Electrospinning technology: designing nanofibers toward wound healing application. In: Nanomaterials-toxicity, human health and environment. IntechOpen, pp 1–19
42. Yao C-H, Lee C-Y, Huang C-H, Chen Y-S, Chen K-Y (2017) Novel bilayer wound dressing based on electrospun gelatin/keratin nanofibrous mats for skin wound repair. Mater Sci Eng C 79:533–540
43. Alotaibi BS, Shoukat M, Buabeid M, Khan AK, Murtaza G (2022) Healing potential of neomycin-loaded electrospun nanofibers against burn wounds. J Drug Deliv Sci Technol 74:103502
44. Hemati Azandaryani A, Derakhshandeh K, Arkan E (2018) Electrospun nanobandage for hydrocortisone topical delivery as an antipsoriasis candidate. Int J Polym Mater Polym Biomater 67(11):677–685
45. Kausar A (2019) Polyacrylonitrile nanocomposite with carbon nanostructures: a review. Polym Plast Technol Mater 58(7):707–731
46. Ullah S, Hashmi M, Kharaghani D, Khan MQ, Saito Y, Yamamoto T, Lee J, Kim IS (2019) Antibacterial properties of in situ and surface functionalized impregnation of silver sulfadiazine in polyacrylonitrile nanofiber mats. Int J Nanomed 14:2693
47. Cancio LC (2021) Topical antimicrobial agents for burn wound care: history and current status. Surg Infect 22(1):3–11
48. Cartotto R (2017) Topical antimicrobial agents for pediatric burns. Burns Trauma 5:21
49. Ono S, Imai R, Ida Y, Shibata D, Komiya T, Matsumura H (2015) Increased wound pH as an indicator of local wound infection in second degree burns. Burns 41(4):820–824
50. Gangwar A, Kumar P, Singh R, Kush P (2021) Recent advances in mupirocin delivery strategies for the treatment of bacterial skin and soft tissue infection. Future Pharmacol 1(1):80–103
51. Seah C, Alexander DC, Louie L, Simor A, Low DE, Longtin J, Melano RG (2012) MupB, a new high-level mupirocin resistance mechanism in Staphylococcus aureus. Antimicrob Agents Chemother 56(4):1916–1920
52. Xu L, Liu Y, Zhou W, Yu D (2022) Electrospun medical sutures for wound healing: a review. Polymers 14(9):1637
53. Zhang W, Ronca S, Mele E (2017) Electrospun nanofibres containing antimicrobial plant extracts. Nanomaterials 7(2):42
54. Avci H, Gergeroglu H (2019) Synergistic effects of plant extracts and polymers on structural and antibacterial properties for wound healing. Polym Bull 76:3709–3731
55. Femi-Adepoju AG, Dada AO, Otun KO, Adepoju AO, Fatoba OP (2019) Green synthesis of silver nanoparticles using terrestrial fern (*Gleichenia Pectinata* (Willd.) *C. Presl*): characterization and antimicrobial studies. Heliyon 5(4):e01543
56. Kumar V, Bano D, Mohan S, Singh DK, Hasan SH (2016) Sunlight-induced green synthesis of silver nanoparticles using aqueous leaf extract of *Polyalthia longifolia* and its antioxidant activity. Mater Lett 181:371–377
57. Huq MA (2020) Green synthesis of silver nanoparticles using *Pseudoduganella eburnea* MAHUQ-39 and their antimicrobial mechanisms investigation against drug resistant human pathogens. Int J Mol Sci 21(4):1510
58. Mendes C, Thirupathi A, Corrêa ME, Gu Y, Silveira PC (2022) The use of metallic nanoparticles in wound healing: new perspectives. Int J Mol Sci 23(23):15376
59. Sellami H, Khan SA, Ahmad I, Alarfaj AA, Hirad AH, Al-Sabri AE (2021) Green synthesis of silver nanoparticles using *Olea europaea* leaf extract for their enhanced antibacterial, antioxidant, cytotoxic and biocompatibility applications. Int J Mol Sci 22(22):12562
60. Das G, Shin H-S, Patra JK (2022) Key health benefits of Korean Ueong dry root extract combined silver nanoparticles. Int J Nanomed 2:4261–4275
61. Srikhao N, Ounkaew A, Srichiangsa N, Phanthanawiboon S, Boonmars T, Artchayasawat A, Theerakulpisut S, Okhawilai M, Kasemsiri P (2022) Green-synthesized silver nanoparticle coating on paper for antibacterial and antiviral applications. Polym Bull 8:1–18

62. Beyene HD, Werkneh AA, Bezabh HK, Ambaye TG (2017) Synthesis paradigm and applications of silver nanoparticles (AgNPs), a review. Sustain Mater Technol 13:18–23

63. Khandel P, Yadaw RK, Soni DK, Kanwar L, Shahi SK (2018) Biogenesis of metal nanoparticles and their pharmacological applications: present status and application prospects. J Nanostruct Chem 8(3):217–254

64. Lee SH, Jun B-H (2019) Silver nanoparticles: synthesis and application for nanomedicine. Int J Mol Sci 20(4):865

65. Roy A, Bulut O, Some S, Mandal AK, Yilmaz MD (2019) Green synthesis of silver nanoparticles: biomolecule-nanoparticle organizations targeting antimicrobial activity. RSC Adv 9(5):2673–2702

66. Fadaka AO, Meyer S, Ahmed O, Geerts G, Madiehe MA, Meyer M, Sibuyi NR (2022) Broad spectrum anti-bacterial activity and non-selective toxicity of gum Arabic silver nanoparticles. Int J Mol Sci 23(3):1799

67. Mohanta YK, Nayak D, Mishra AK, Chakrabartty I, Ray MK, Mohanta TK, Tayung K, Rajaganesh R, Vasanthakumaran M, Muthupandian S (2022) Green synthesis of endolichenic fungi functionalized silver nanoparticles: the role in antimicrobial, anti-cancer, and mosquitocidal activities. Int J Mol Sci 23(18):10626

68. Nicolae-Maranciuc A, Chicea D, Chicea LM (2022) Ag nanoparticles for biomedical applications—synthesis and characterization—a review. Int J Mol Sci 23(10):5778

69. Shkryl Y, Rusapetova T, Yugay Y, Egorova A, Silantev V, Grigorchuk V, Karabtsov A, Timofeeva Y, Vasyutkina E, Kudinova O (2021) Biosynthesis and cytotoxic properties of ag, au, and bimetallic nanoparticles synthesized using *Lithospermum erythrorhizon* callus culture extract. Int J Mol Sci 22(17):9305

70. Alvandi H, Rajati H, Naseriyeh T, Rahmatabadi SS, Hosseinzadeh L, Arkan E (2023) Incorporation of *Aloe vera* and green synthesized ZnO nanoparticles into the chitosan/PVA nanocomposite hydrogel for wound dressing application. Polym Bull 8:1–26

71. Jadhav K, Dhamecha D, Bhattacharya D, Patil M (2016) Green and ecofriendly synthesis of silver nanoparticles: characterization, biocompatibility studies and gel formulation for treatment of infections in burns. J Photochem Photobiol B 155:109–115

72. Jain AS, Pawar PS, Sarkar A, Junnuthula V, Dyawanapelly S (2021) Bionanofactories for green synthesis of silver nanoparticles: toward antimicrobial applications. Int J Mol Sci 22(21):11993

73. Nematpour N, Moradipour P, Zangeneh MM, Arkan E, Abdoli M, Behbood L (2020) The application of nanomaterial science in the formulation a novel antibiotic: assessment of the antifungal properties of mucoadhesive clotrimazole loaded nanofiber versus vaginal films. Mater Sci Eng C 110:110635

74. Venkatesan J, Kim S-K, Shim MS (2016) Antimicrobial, antioxidant, and anticancer activities of biosynthesized silver nanoparticles using marine algae *Ecklonia cava*. Nanomaterials 6(12):235

75. Ogli Juraev SS, Madrakhimova SD, Tashpulatov FN, Ogli Esanov RS, Matchanov AD (2020) The study of the micronutrient composition of the plant *Capsella bursa-pastoris*, growing in mountainous areas. Am J Appl Sci 2(09):207–220

76. Rembe J-D, Fromm-Dornieden C, Stuermer EK (2018) Effects of vitamin B complex and vitamin C on human skin cells: is the perceived effect measurable? Adv Skin Wound Care 31(5):225–233

77. Bussmann RW, Batsatsashvili K, Kikvidze Z, Khajoei Nasab F, Ghorbani A, Paniagua-Zambrana NY, Khutsishvili M, Maisaia I, Sikharulidze S, Tchelidze D (2020) *Capsella bursa-pastoris* (L.) *Medik brassicaceae*. Ethnobotany of the Mountain Regions of Far Eastern Europe: Ural, Northern Caucasus, Turkey, and Iran, pp 1–10

78. Grosso C, Vinholes J, Silva LR, Pinho PGD, Gonçalves RF, Valentão P, Jäger AK, Andrade PB (2011) Chemical composition and biological screening of *Capsella bursa-pastoris*. Rev Bras 21:635–643

79. Darvishi E, Kahrizi D, Arkan E (2019) Comparison of different properties of zinc oxide nanoparticles synthesized by the green (using *Juglans regia* L. leaf extract) and chemical methods. J Mol Liq 286:110831

80. Pirtarighat S, Ghannadnia M, Baghshahi S (2019) Green synthesis of silver nanoparticles using the plant extract of *Salvia spinosa* grown in vitro and their antibacterial activity assessment. J Nanostruct Chem 9(1):1–9

81. Jalilian F, Chahardoli A, Sadrjavadi K, Fattahi A, Shokoohinia Y (2020) Green synthesized silver nanoparticle from *Allium ampeloprasum* aqueous extract: characterization, antioxidant activities, antibacterial and cytotoxicity effects. Adv Powder Technol 31(3):1323–1332

82. Jayapriya M, Dhanasekaran D, Arulmozhi M, Nandhakumar E, Senthilkumar N, Sureshkumar K (2019) Green synthesis of silver nanoparticles using piper longum catkin extract irradiated by sunlight: antibacterial and catalytic activity. Res Chem Intermed 45(6):3617–3631

83. Prathna T, Raichur AM, Chandrasekaran N, Mukherjee A (2014) Sunlight irradiation induced green synthesis of stable silver nanoparticles using citrus limon extract. Proc Natl Acad Sci India Sect B Biol Sci 84(1):65–70

84. Singh J, Mehta A, Rawat M, Basu S (2018) Green synthesis of silver nanoparticles using sun dried tulsi leaves and its catalytic application for 4-nitrophenol reduction. J Environ Chem Eng 6(1):1468–1474

85. Peng YY, Glattauer V, Ramshaw JA (2017) Stabilisation of collagen sponges by glutaraldehyde vapour crosslinking. Int J Biomater

86. Balouiri M, Sadiki M, Ibnsouda SK (2016) Methods for in vitro evaluating antimicrobial activity: a review. J Pharmaceut Anal 6(2):71–79

87. Parvekar P, Palaskar J, Metgud S, Maria R, Dutta S (2020) The minimum inhibitory concentration (MIC) and minimum bactericidal concentration (MBC) of silver nanoparticles against Staphylococcus aureus. Biomater Investig Dent 7(1):105–109

88. Li X, Wang C, Yang S, Liu P, Zhang B (2018) Electrospun PCL/mupirocin and chitosan/lidocaine hydrochloride multifunctional double layer nanofibrous scaffolds for wound dressing applications. Int J Nanomed 13:5287

89. Li C, Fu R, Yu C, Li Z, Guan H, Hu D, Zhao D, Lu L (2013) Silver nanoparticle/chitosan oligosaccharide/poly(vinyl alcohol) nanofibers as wound dressings: a preclinical study. Int J Nanomed 8:4131

90. Allafchian A, Hosseini H, Ghoreishi SM (2020) Electrospinning of PVA-carboxymethyl cellulose nanofibers for flufenamic acid drug delivery. Int J Biol Macromol 163:1780–1786

91. Guo X, Liu Y, Bera H, Zhang H, Chen Y, Cun D, Fodera V, Yang M (2020) α-Lactalbumin-based nanofiber dressings improve burn wound healing and reduce scarring. ACS Appl Mater Interfaces 12(41):45702–45713

92. Hadisi Z, Farokhi M, Bakhsheshi-Rad HR, Jahanshahi M, Hasanpour S, Pagan E, Dolatshahi-Pirouz A, Zhang YS, Kundu SC, Akbari M (2020) Hyaluronic acid (HA)-based silk fibroin/zinc oxide core–shell electrospun dressing for burn wound management. Macromol Biosci 20(4):1900328

93. Bhatnagar S, Kobori T, Ganesh D, Ogawa K, Aoyagi H (2019) Biosynthesis of silver nanoparticles mediated by extracellular pigment from *Talaromyces purpurogenus* and their biomedical applications. Nanomaterials 9(7):1042

94. Allafchian A, Mirahmadi-Zare S, Jalali S, Hashemi S, Vahabi M (2016) Green synthesis of silver nanoparticles using phlomis leaf extract and investigation of their antibacterial activity. J Nanostruct. Chem. 6(2):129–135

95. Erci F, Cakir-Koc R, Isildak I (2018) Green synthesis of silver nanoparticles using *Thymbra spicata* L. var spicata (zahter) aqueous leaf extract and evaluation of their morphology-dependent antibacterial and cytotoxic activity. Artif Cells Nanomed Biotechnol 46(sup1):150–158

96. Geană E-I, Ciucure CT, Apetrei C, Artem V (2019) Application of spectroscopic UV-Vis and FT-IR screening techniques coupled with multivariate statistical analysis for red wine authentication: varietal and vintage year discrimination. Molecules 24(22):4166

97. Domínguez AV, Algaba RA, Canturri AM, Villodres ÁR, Smani Y (2020) Antibacterial activity of colloidal silver against gram-negative and gram-positive bacteria. Antibiotics 9:1

98. Hosnedlova B, Kabanov D, Kepinska M, Narayanan VHB, Parikesit AA, Fernandez C, Bjørklund G, Nguyen HV, Farid A, Sochor J (2022) Effect of Biosynthesized silver nanoparticles on bacterial biofilm changes in *S. aureus* and *E. coli*. Nanomaterials 12(13):2183

99. Liu C, Shen J, Yeung KWK, Tjong SC (2017) Development and antibacterial performance of novel polylactic acid-graphene oxide-silver nanoparticle hybrid nanocomposite mats prepared by electrospinning. ACS Biomater Sci Eng 3(3):471–486

100. Pan S-F, Ke X-X, Wang T-Y, Liu Q, Zhong L-B, Zheng Y-M (2018) Synthesis of silver nanoparticles embedded electrospun PAN nanofiber thin-film composite forward osmosis membrane to enhance performance and antimicrobial activity. Ind Eng Chem Res 58(2):984–993

101. Sichani GN, Morshed M, Amirnasr M, Abedi D (2010) In situ preparation, electrospinning, and characterization of polyacrylonitrile nanofibers containing silver nanoparticles. J Appl Polym Sci 116(2):1021–1029

102. Cai S, Wu C, Yang W, Liang W, Yu H, Liu L (2020) Recent advance in surface modification for regulating cell adhesion and behaviors. Nanotechnol Rev 9(1):971–989

103. Kong Y, Tang X, Zhao Y, Chen X, Yao K, Zhang L, Han Q, Zhang L, Ling J, Wang Y (2020) Degradable tough chitosan dressing for skin wound recovery. Nanotechnol Rev 9(1):1576–1585

104. Paarakh MP, Jose PA, Setty C, Christoper G (2018) Release kinetics-concepts and applications. Int J Pharm Res Technol 8(1):12–20

105. Dong X, Mitchell DG, Cervantes MYG, Chitara B, Yang L, Yan F (2022) Rose bengal-integrated electrospun polyacrylonitrile nanofibers for photodynamic inactivation of bacteria. Environ Sci Adv 1(5):736–745

106. Weng L, Xie J (2015) Smart electrospun nanofibers for controlled drug release: recent advances and new perspectives. Curr Pharm Des 21(15):1944–1959

107. Kharaghani D, Jo YK, Khan MQ, Jeong Y, Cha HJ, Kim IS (2018) Electrospun antibacterial poly-acrylonitrile nanofiber membranes functionalized with silver nanoparticles by a facile wetting method. Eur Polym J 108:69–75

108. Su K, Wang C (2015) Recent advances in the use of gelatin in biomedical research. Biotech Lett 37(11):2139–2145

109. Szabo P, Zelko R (2015) Formulation and stability aspects of nanosized solid drug delivery systems. Curr Pharm Des 21(22):3148–3157

110. Karami Z, Rezaeian I, Zahedi P, Abdollahi M (2013) Preparation and performance evaluations of electrospun poly(ε-caprolactone), poly(lactic acid), and their hybrid (50/50) nanofibrous mats containing thymol as an herbal drug for effective wound healing. J Appl Polym Sci 129(2):756–766

111. Akia M, Rodriguez C, Materon L, Gilkerson R, Lozano K (2019) Antibacterial activity of polymeric nanofiber membranes impregnated with Texas sour orange juice. Eur Polym J 115:1–5

112. Tan ST, Dosan R (2019) Lessons from epithelialization: the reason behind moist wound environment. Open Dermatol J 13:1

Authors and Affiliations

Rozhin Karami[1] · Pouran Moradipour[2,3] · Elham Arkan[3] · Reza Zarghami[1] · Khodabakhsh Rashidi[4] · Elahe Darvishi[5]

✉ Reza Zarghami
rzarghami@ut.ac.ir

1 Pharmaceutical Engineering Research Laboratory, Pharmaceutical Process Center of Excellence, School of Chemical Engineering, University of Tehran, P.O. Box 11155/4563, Tehran, Iran

2 School of Chemical Engineering, College of Engineering, University of Tehran, Tehran, Iran

3 Nano-Drug Delivery Research Center, Institute of Health Technology, Kermanshah University of Medical Sciences, Kermanshah, Iran

4 Research Center of Oils & Fat, Food and Drug Administration, Kermanshah, Iran

5 Department of Nanobiotechnology, Faculty of Biotechnology, Amol University of Special Modern Technologies, Amol, Iran